

Helium nuclei, deuteron and dineutron in 2+1 flavor lattice QCD

Takeshi Yamazaki,^{1,2} Ken-ichi Ishikawa,^{3,2} Yoshinobu Kuramashi,^{4,5,2} and Akira Ukawa⁴

¹*Kobayashi-Maskawa Institute for the Origin of Particles and the Universe,*

Nagoya University, Naogya, Aichi 464-8602, Japan

²*RIKEN Advanced Institute for Computational Science, Kobe, Hyogo 650-0047, Japan*

³*Department of Physics, Hiroshima University,*

Higashi-Hiroshima, Hiroshima 739-8526, Japan

⁴*Center for Computational Sciences,*

University of Tsukuba, Tsukuba, Ibaraki 305-8577, Japan

⁵*Graduate School of Pure and Applied Sciences,*

University of Tsukuba, Tsukuba, Ibaraki 305-8571, Japan

(Dated: July 19, 2012)

Abstract

We calculate the binding energies for multi-nucleon bound states with the nuclear mass number less than or equal to 4 in 2+1 flavor QCD at the lattice spacing of $a = 0.09$ fm employing a relatively heavy quark mass corresponding to $m_\pi = 0.51$ GeV. To distinguish a bound state from attractive scattering states, we investigate the volume dependence of the energy shift between the ground state and the state of free nucleons by changing the spatial extent of the lattice from 2.9 fm to 5.8 fm. We conclude that ${}^4\text{He}$, ${}^3\text{He}$, deuteron and dineutron are bound at $m_\pi = 0.51$ GeV. We compare their binding energies with those in our quenched studies and also with several previous investigations.

PACS numbers: 11.15.Ha, 12.38.Aw, 12.38.-t 12.38.Gc

I. INTRODUCTION

Lattice QCD has a potential ability to quantitatively understand the nature of nuclei, whose characteristic feature is a hierarchical structure in the strong interaction. The nuclear binding energy is experimentally known to be about 10 MeV per nucleon, which is much smaller than the typical energy scale of hadrons. A measurement of the binding energies is therefore the first step for direct investigation of nuclei in lattice QCD. A key ingredient in the study is a systematic change of the spatial volume of the lattice to distinguish a bound state from an attractive scattering state.

We carried out a first attempt to measure the binding energies of the ^4He and ^3He nuclei in quenched QCD with a rather heavy quark mass corresponding to $m_\pi = 0.80$ GeV, thereby avoiding heavy computational cost [1]. We followed this work by a renewed investigation of the bound state for the two-nucleon channel in quenched QCD at the same quark mass, which found that not only the deuteron in the $^3\text{S}_1$ channel but also the dineutron in the $^1\text{S}_0$ channel is bound [2]. Independently, NPLQCD collaboration reported the possibility that a bound state is formed in both channels at $m_\pi = 0.39$ GeV in 2+1 flavor QCD [3]. They later confirmed the bound states for the helium nuclei and the two-nucleon channels at $m_\pi = 0.81$ GeV in 3-flavor QCD taking a different choice for the quark and gluon actions [4].

In this article we report on our investigation of the dynamical quark effects on the binding energies of the helium nuclei, the deuteron and the dineutron. We perform 2+1 flavor lattice QCD simulation with the degenerate up and down quark mass corresponding to $m_\pi = 0.51$ GeV. Four lattice sizes are employed to take the infinite spatial volume limit: $32^3 \times 48$, $40^3 \times 48$, $48^3 \times 48$ and $64^3 \times 64$, whose spatial extent ranges from 2.9 fm to 5.8 fm with the lattice spacing of $a = 0.08995(40)$ fm [5].

For the helium nuclei our main interest lies in the magnitude of the binding energies, since all studies carried out so far, both in quenched and in unquenched QCD and for several quark mass values, agree on the bound state nature for helium nuclei. Much more intriguing is the two-nucleon system, for which there are two ways to study. One is a direct investigation [2–4, 6–9] in which one calculates the two-nucleon Green's functions directly in lattice QCD, and the other is an indirect calculation by means of the two-nucleon effective potential extracted from the two-nucleon wave function in lattice QCD [10, 11].

So far only the former method has reported the binding energies of the two-nucleon

systems. In quenched QCD the bound state nature has been confirmed for both channels at $m_\pi = 0.80$ GeV in our recent work [2]. On the other hand, unquenched studies show a complicated situation. A somewhat early study in 2+1 flavor QCD with a mixed action [8] reported a positive energy shift (repulsive interaction) in both channels at $m_\pi \leq 0.59$ GeV. More recently, however, deep bound states were observed at $m_\pi = 0.81$ GeV in 3-flavor QCD [4]. We hope to shed light on this situation with our own investigation in 2+1 flavor QCD.

This paper is organized as follows. In Sec. II we explain simulation details including the simulation parameters and the interpolating operators for the multi-nucleon channels. Section III presents the results of the binding energies for the helium nuclei, the deuteron and the dineutron. We compare our results with those in the previous studies. Conclusions and discussions are summarized in Sec. IV.

II. SIMULATION DETAILS

A. Simulation parameters

We generate 2+1 flavor gauge configurations with the Iwasaki gauge action [12] and the non-perturbative $O(a)$ -improved Wilson quark action at $\beta = 1.90$ with $c_{\text{SW}} = 1.715$ [13]. The lattice spacing is $a = 0.8995(40)$ fm, corresponding to $a^{-1} = 2.194(10)$ GeV, determined with $m_\Omega = 1.6725$ GeV [5]. We take four lattice sizes, $L^3 \times T = 32^3 \times 48$, $40^3 \times 48$, $48^3 \times 48$ and $64^3 \times 64$, to investigate the spatial volume dependence of the ground state energy shift between the multi-nucleon system and the free nucleons. The physical spatial extents are 2.9, 3.6, 4.3 and 5.8 fm, respectively. Since it becomes harder to obtain a good signal-to-noise ratio at lighter quark masses for multi-nucleon systems [7, 14], we employ the hopping parameters $(\kappa_{ud}, \kappa_s) = (0.1373316, 0.1367526)$ which correspond to $m_\pi = 0.51$ GeV and $m_N = 1.32$ GeV and the physical value for the strange quark mass. These values are chosen based on the previous results for m_π and m_s obtained by the PACS-CS Collaboration [5, 15].

We employ the domain-decomposed Hybrid-Monte-Carlo (DDHMC) algorithm [16, 17] for the degenerate light quarks and the UV-filtered PHMC (UVPHMC) algorithm [18] for the strange quark employing the Omelyan-Mryglod-Folk integrator [19, 20]. The algorithmic details are given in Ref. [15]. We summarize simulation parameters in Table I including the

block sizes in DDHMC and the polynomial order in UVPHMC. We take $\tau = 1$ for the trajectory length of the molecular dynamics in all the runs. The step sizes are chosen such that we obtain reasonable acceptance rates presented in Table I. We generate the gauge configurations in a single run except for the $L = 64$ case for which we carry out two runs. The total trajectory length is about 2000 for all the volumes, except 4000 for the case of smallest volume.

B. Calculation method

We extract the ground state energies of the multi-nucleon systems and the nucleon state from the correlation functions

$$G_{\mathcal{O}}(t) = \langle 0 | \mathcal{O}(t) \overline{\mathcal{O}}(0) | 0 \rangle \quad (1)$$

with \mathcal{O} being appropriate operators for ${}^4\text{He}$, ${}^3\text{He}$, two-nucleon ${}^3\text{S}_1$ and ${}^1\text{S}_0$ channels, and the nucleon state N (see the next subsection for actual expressions).

We carry out successive measurements in the interval of 10 trajectories. The errors are estimated by jackknife analysis choosing 200 trajectories for the bin size for all volumes, except for the largest volume for which we use 190. The numbers of configurations are listed in Table II. We attempt to extract as much information as possible from each configuration by repeating the measurement of the correlation functions for a number of sources at different spatial points and time slices. For the 48^4 and 64^4 lattices, we calculate the correlation functions not only in the temporal direction but also in the three spatial directions exploiting the space-time rotational symmetry. We found that this procedure effectively increases statistics by a factor of four. This factor is included in the number of measurements on each configuration given in Table II

We are interested in the energy shift between the ground state of the multi-nucleon system and the free nucleons on an L^3 box,

$$\Delta E_L = E_{\mathcal{O}} - N_N m_N \quad (2)$$

with $E_{\mathcal{O}}$ being the lowest energy level for the multi-nucleon channel, N_N the number of nucleon and m_N the nucleon mass. This quantity is directly extracted from the ratio of the multi-nucleon correlation function divided by the N_N -th power of the nucleon correlation

function

$$R(t) = \frac{G_{\mathcal{O}}(t)}{(G_N(t))^{N_N}}, \quad (3)$$

where the same source operator is chosen for the numerator and the denominator. We also define the effective energy shift as

$$\Delta E_L^{\text{eff}} = \ln \left(\frac{R(t)}{R(t+1)} \right), \quad (4)$$

which is useful to check the plateau region in later sections.

Note that the definitions for ΔE_L and ΔE_L^{eff} follow those in Ref. [2], but are opposite to those used in Ref. [1].

C. Interpolating operators

We use an interpolating operator for the proton given by

$$p_\alpha = \varepsilon_{abc}([u_a]^t C \gamma_5 d_b) u_c^\alpha, \quad (5)$$

where $C = \gamma_4 \gamma_2$ and α and a, b, c are the Dirac index and the color indices, respectively. The neutron operator n_α is obtained by replacing u_c^α by d_c^α in the proton operator. To save the computational cost we use the non-relativistic quark operator, in which the Dirac index is restricted to the upper two components.

The ${}^4\text{He}$ nucleus has zero total angular momentum, positive parity $J^P = 0^+$ and zero isospin $I = 0$. We employ the simplest ${}^4\text{He}$ interpolating operator with zero orbital angular momentum $L = 0$, and hence $J = S$ with S being the total spin. Such an operator was already given long time ago in Ref. [21],

$${}^4\text{He} = \frac{1}{\sqrt{2}} (\bar{\chi} \eta - \chi \bar{\eta}), \quad (6)$$

where

$$\chi = \frac{1}{2} ([+-+ -] + [-+ -+] - [+ - -+] - [-+ + -]), \quad (7)$$

$$\bar{\chi} = \frac{1}{\sqrt{12}} ([+ - + -] + [- + -+] + [+ - -+] + [- + + -] - 2[+ + - -] - 2[- - + +]) \quad (8)$$

with $+/-$ being up/down spin of each nucleon, and $\eta, \bar{\eta}$ are obtained by replacing $+/-$ in $\chi, \bar{\chi}$ by p/n for the isospin. Each nucleon in the sink operator is projected to zero spatial momentum.

We also calculate the correlation function of the ^3He nucleus whose quantum numbers are $J^P = \frac{1}{2}^+$, $I = \frac{1}{2}$ and $I_z = \frac{1}{2}$. We employ the interpolating operator in Ref. [22],

$$^3\text{He} = \frac{1}{\sqrt{6}} (|p_- n_+ p_+\rangle - |p_+ n_+ p_-\rangle + |n_+ p_+ p_-\rangle - |n_+ p_- p_+\rangle + |p_+ p_- n_+\rangle - |p_- p_+ n_+\rangle), \quad (9)$$

with the zero momentum projection on each nucleon in the sink operator.

The two-nucleon operators for the $^3\text{S}_1$ and $^1\text{S}_0$ channels are given by

$$NN_{^3\text{S}_1}(t) = \frac{1}{\sqrt{2}} [p_+(t)n_+(t) - n_+(t)p_+(t)], \quad (10)$$

$$NN_{^1\text{S}_0}(t) = \frac{1}{\sqrt{2}} [n_+(t)n_-(t) - n_-(t)n_+(t)]. \quad (11)$$

In the spin triplet channel the operators for the other two spin components are constructed in a similar way. We take average over the three spin components.

The quark propagators are solved with the periodic boundary condition in all the spatial and temporal directions using the exponentially smeared source of form

$$q'(\vec{x}, t) = \sum_{\vec{y}} A e^{-B|\vec{x}-\vec{y}|} q(\vec{y}, t) \quad (12)$$

after the Coulomb gauge fixing. We choose the smearing parameters depending on the volume (see Table II) in order to obtain reasonable plateaux of the effective energy for the ground states in the multi-nucleon channels as well as for the nucleon. For the source operators explained above we insert the *smeared* quark fields of Eq. (12) for each nucleon operator located at the same spatial point \vec{x} . Each nucleon in the sink operator, on the other hand, is composed of the *point* quark fields, and projected to zero spatial momentum.

D. Difficulties for multi-nucleon channel

There are several computational difficulties in the calculation of the correlation functions $G_{\mathcal{O}}(t)$ for the ^3He and ^4He channels. One is a factorially large number of Wick contractions for the quark-antiquark fields. A naive counting gives $(2N_p + N_n)!(2N_n + N_p)!$ for a nucleus composed of N_p protons and N_n neutrons, which quickly becomes prohibitively large beyond three-nucleon systems, *e.g.*, 2,880 for ^3He and 518,400 for ^4He . To overcome the difficulty, we use the reduction techniques proposed in our exploratory work [1]. After the reduction, only 1107 (93) contractions are required for the correlation function in the ^4He (^3He) channel.

Other reduction techniques for the large number of the Wick contractions have been proposed for the multi-meson [23] and multi-baryon [24, 25] channels.

Another difficulty in studying a multi-nucleon bound state is the identification of the bound state nature in a finite volume, because an attractive scattering state yields a similar energy shift due to the finite volume effect [26–28]. To solve the problem we need to investigate the volume dependence of the measured energy shift [1, 2]: For a scattering state, the energy shift decreases in proportion to $1/L^3$ at the leading order in the $1/L$ expansion [26, 29], while for a bound state the energy shift remains at a finite value in the infinite spatial volume limit. In order to distinguish a non-zero constant from a $1/L^3$ behavior in the energy shift, we employ four spatial extents from 2.9 to 5.8 fm.

III. RESULTS

A. Nucleon

We first show the effective nucleon mass on the $(5.8 \text{ fm})^3$ box in Fig. 1 as a typical result. The plateau of the effective mass is clearly observed. A fit result of the correlation function with an exponential form is also drawn in the figure with the one standard deviation error band. We list the nucleon mass together with the pion mass in Table II.

B. ^4He nucleus

The effective energy shift ΔE_L^{eff} defined in Eq. (4) is plotted in Fig. 2. The signal is clear up to $t = 12$, beyond which the statistical error increases rapidly. The energy shift ΔE_L is extracted from $R(t)$ of Eq. (3) by an exponential fit over the range of $t = 10\text{--}14$. The fit result is denoted by the solid lines with the statistical error band in Fig. 2. The systematic error in the fit is estimated from the variation of the fit results with the minimum or maximum time slice changed by ± 1 . Results with similar quality are obtained on other volumes. We summarize the values of ΔE_L with the statistical and systematic errors in Table III.

Figure 3 shows the volume dependence of ΔE_L as a function of $1/L^3$. The inner bar denotes the statistical error and the outer bar represents the statistical and systematic errors

combined in quadrature. The negative energy shifts are obtained in all the four volumes. We extrapolate the results to the infinite volume limit with a simple linear function of $1/L^3$,

$$\Delta E_L = \Delta E_\infty + \frac{C_L}{L^3}. \quad (13)$$

The systematic error is estimated from the variation of the results obtained by alternative fits which contains a constant fit of the data and a fit of the data obtained with a different fit range in t . The non-zero negative value obtained for the infinite volume limit ΔE_∞ shown in Fig. 3 and Table III leads us to conclude that the ground state is bound in this channel for the quark masses employed. The binding energy $-\Delta E_\infty = 43(12)(8)$ MeV, where the first error is statistical and the second one is systematic, is consistent with the experimental result of 28.3 MeV and also with the previous quenched result at $m_\pi = 0.80$ GeV [2]. Note that the error is still quite large.

A recent work in 3-flavor QCD at $m_\pi = 0.81$ GeV reported a value 110(20)(15) MeV for the binding energy of ^4He nucleus [4]. This is about three times deeper than our value. Whether this difference can be attributed to the quark mass dependence in unquenched calculations needs to be clarified in future.

C. ^3He nucleus

Figure 4 shows the effective energy shift ΔE_L^{eff} of Eq. (4). The quality of the signal is better than the ^4He channel in Fig. 2. An exponential fit of $R(t)$ in Eq. (3) with the range of $t = 9\text{--}14$ yields a negative value, which is denoted by the solid lines with the statistical error band in Fig. 4. The systematic error in the fit is estimated in the same way as in the ^4He case.

As listed in Table III we find non-zero negative values for the energy shift ΔE_L for all the volumes. The volume dependence is illustrated in Fig. 5 as a function of $1/L^3$ with the inner and outer error bars as explained in the previous subsection. We carry out a linear extrapolation of Eq. (13). The systematic error is estimated in the same way as in the ^4He channel. The energy shift extrapolated to the infinite spatial volume limit is non-zero and negative, see Fig. 5 and Table III, which means that the ground state is a bound state in this channel. The value of $-\Delta E_\infty = 20.3(4.0)(2.0)$ MeV is roughly three times larger than the experimental result, 7.72 MeV, though consistent with our previous quenched result at

$m_\pi = 0.80$ GeV [2].

In 3-flavor QCD $-\Delta E_\infty = 71(6)(5)$ MeV was reported [4] at a heavier quark mass corresponding to $m_\pi = 0.81$ GeV. Here again future work is needed to see if a quark mass dependence explains the difference from the experiment.

D. Two-nucleon channels

1. Present work

In Fig. 6 we show the time dependence for ΔE_L^{eff} of Eq. (4) in the $^3\text{S}_1$ channel. The signals are lost beyond $t \approx 14$. We observe negative values beyond the error bars in the plateau region of $t = 9$ –14. We extract the value of ΔE_L from an exponential fit for $R(t)$ of Eq. (3) in the range of $t = 9$ –14. The systematic error of the fit is estimated as explained in the previous subsections.

Figure 7 shows the result for ΔE_L^{eff} in the $^1\text{S}_0$ channel on the $(5.8 \text{ fm})^3$ box. The value of ΔE_L^{eff} is again negative beyond the error bars in the plateau region, though the absolute value is smaller than in the $^3\text{S}_1$ case. The energy shift ΔE_L is obtained in the same way as for the $^3\text{S}_1$ channel.

The volume dependences of ΔE_L in the $^3\text{S}_1$ and $^1\text{S}_0$ channels are plotted as a function of $1/L^3$ in Figs. 8 and 9, respectively. The numerical values of ΔE_L on all the spatial volumes are summarized in Table IV, where the statistical and systematic errors are given in the first and second parentheses, respectively. There is little volume dependence for ΔE_L , indicating a non-zero negative value in the infinite volume and a bound state, rather than the $1/L^3$ dependence expected for a scattering state, for the ground state for both channels.

The binding energies in the infinite spatial volume limit in Table IV are obtained by fitting the data with a function including a finite volume effect on the two-particle bound state [27, 28],

$$\Delta E_L = -\frac{\gamma^2}{m_N} \left\{ 1 + \frac{C_\gamma}{\gamma L} \sum'_{\vec{n}} \frac{\exp(-\gamma L \sqrt{\vec{n}^2})}{\sqrt{\vec{n}^2}} \right\}, \quad (14)$$

where γ and C_γ are free parameters, \vec{n} is three-dimensional integer vector, and $\sum'_{\vec{n}}$ denotes the summation without $|\vec{n}| = 0$. The binding energy $-\Delta E_\infty$ is determined from

$$-\Delta E_\infty = \frac{\gamma^2}{m_N}, \quad (15)$$

where we assume

$$2\sqrt{m_N^2 - \gamma^2} - 2m_N \approx -\frac{\gamma^2}{m_N}. \quad (16)$$

The systematic error is estimated from the variation of the fit results choosing different fit ranges in the determination of ΔE_L and also using constant and linear fits as an alternative fit forms. We obtain the binding energies $-\Delta E_\infty = 11.5(1.1)(0.6)$ MeV and $7.4(1.3)(0.6)$ MeV for the 3S_1 and 1S_0 channels, respectively. The result for the 3S_1 channel is roughly five times larger than the experimental value, 2.22 MeV. Our finding of a bound state in the 1S_0 channel contradicts the experimental observation. These features are consistent with our quenched results with a heavy quark mass corresponding to $m_\pi = 0.80$ GeV [2].

2. Comparison with previous studies

A number of studies have been performed for the two-nucleon channel after the first work of Ref. [7]. It is therefore instructive to summarize the results and make a comparison with each other. Table V tabulates, in chronological order, the results for $-\Delta E_L$ for the 3S_1 and 1S_0 channels together with the pion mass m_π and the spatial extent L in physical units. The numbers are plotted in Figs. 10 and 11 for the 3S_1 and 1S_0 channels, respectively, as a function of m_π^2 .

The early studies in Refs. [7, 8, 11] employed a single volume, and we do not observe a common feature or trend among them. The positive values for $-\Delta E_L$ in Ref. [8] means repulsive interaction for both channels, which is not seen in other studies. The results for $-\Delta E_L$ in Ref. [11] is an order of magnitude smaller compared to other groups, probably due to significant contamination from excited states.

The four recent studies [2–4] have made a systematic investigation of the spatial volume dependence. Our quenched and 2+1 flavor results show qualitatively the same feature that the binding energy for the 3S_1 channel is much larger than the experimental value and the bound state is observed in the 1S_0 channel. The 2+1 flavor results from Ref. [3, 4] at $m_\pi = 0.39$ GeV give non-zero negative values for ΔE_L in both channels on the $\leq (3.9 \text{ fm})^3$ box, which are consistent with our results as shown in Table V. Unfortunately, the extrapolation to the infinite spatial volume limit introduces large errors so that ΔE_∞ becomes consistent with zero within the error bars. The most recent study [4] worked at a heavier quark mass of $m_\pi = 0.81$ GeV in 3-flavor QCD, and found large values for the binding energies: $25(3)(2)$

MeV for the 3S_1 channel and 19(3)(1) MeV for the 1S_0 channel [4]. While all recent studies are consistent with a bound ground state for both 3S_1 and 1S_0 channels when quark masses are heavy, quantitative details still need to be clarified.

IV. CONCLUSION AND DISCUSSION

We have calculated the binding energies for the helium nuclei, the deuteron and the dineutron in 2+1 flavor QCD with $m_\pi = 0.51$ GeV and $m_N = 1.32$ GeV. The bound states are distinguished from the attractive scattering states by investigating the spatial volume dependence of the energy shift ΔE_L . In the infinite spatial volume limit we obtain

$$-\Delta E_\infty = \begin{cases} 43(12)(8) & \text{MeV for } ^4\text{He}, \\ 20.3(4.0)(2.0) & \text{MeV for } ^3\text{He}, \\ 11.5(1.1)(0.6) & \text{MeV for } ^3S_1, \\ 7.4(1.3)(0.6) & \text{MeV for } ^1S_0. \end{cases} \quad (17)$$

While the binding energy for the ^4He nucleus is comparable with the experimental value, those for the ^3He nucleus and the deuteron are much larger than the experimental ones. Furthermore we detect the bound state in the 1S_0 channel as in the previous study with quenched QCD, which is not observed in nature. These findings and the enhanced binding energies at $m_\pi = 0.81$ GeV in 3-flavor QCD [4] tell us that a next step of primary importance is to reduce the up-down quark mass toward the physical values. A possible scenario in the two-nucleon channels is as follows. The binding energy in both channels diminishes monotonically as the up-down quark mass decreases. At some point of the up-down quark mass the binding energy in the 1S_0 channel vanishes and the bound state evaporates into the attractive scattering state, while the binding energy in the 3S_1 channel remains finite up to the physical point. This is a dynamical question on the strong interaction, and only lattice QCD could answer it.

Acknowledgments

Numerical calculations for the present work have been carried out on the HA8000 cluster system at Information Technology Center of the University of Tokyo, on the PACS-CS

computer under the “Interdisciplinary Computational Science Program” of Center for Computational Sciences in University of Tsukuba, on the T2K-Tsukuba cluster system and HA-PACS system at University of Tsukuba, and on K computer at RIKEN Advanced Institute for Computational Science. We thank our colleagues in the PACS-CS Collaboration for helpful discussions and providing us the code used in this work. This work is supported in part by Grants-in-Aid for Scientific Research from the Ministry of Education, Culture, Sports, Science and Technology (Nos. 18104005, 18540250, 22244018) and Grants-in-Aid of the Japanese Ministry for Scientific Research on Innovative Areas (Nos. 20105002, 21105501, 23105708).

-
- [1] T. Yamazaki, Y. Kuramashi, and A. Ukawa (PACS-CS Collaboration), Phys.Rev. **D81**, 111504 (2010).
 - [2] T. Yamazaki, Y. Kuramashi, and A. Ukawa, Phys. Rev. **D84**, 054506 (2011).
 - [3] S. Beane et al. (NPLQCD Collaboration), Phys. Rev. **D85**, 054511 (2012).
 - [4] S. Beane et al. (NPLQCD Collaboration) (2012), arXiv:1206.5219 [hep-lat].
 - [5] S. Aoki et al. (PACS-CS Collaboration), Phys. Rev. **D81**, 074503 (2010).
 - [6] M. Fukugita, Y. Kuramashi, H. Mino, M. Okawa, and A. Ukawa, Phys. Rev. Lett. **73**, 2176 (1994).
 - [7] M. Fukugita, Y. Kuramashi, M. Okawa, H. Mino, and A. Ukawa, Phys. Rev. **D52**, 3003 (1995).
 - [8] S. R. Beane, P. F. Bedaque, K. Orginos, and M. J. Savage, Phys. Rev. Lett. **97**, 012001 (2006).
 - [9] S. R. Beane et al. (NPLQCD), Phys. Rev. **D81**, 054505 (2010).
 - [10] N. Ishii, S. Aoki, and T. Hatsuda, Phys. Rev. Lett. **99**, 022001 (2007).
 - [11] S. Aoki, T. Hatsuda, and N. Ishii, Prog.Theor.Phys. **123**, 89 (2010).
 - [12] Y. Iwasaki (2011), arXiv:1111.7054 [hep-lat].
 - [13] S. Aoki et al. (CP-PACS/JLQCD Collaborations), Phys. Rev. **D73**, 034501 (2006).
 - [14] G. P. Lepage (1989), CLNS-89-971, C89-06-04.
 - [15] S. Aoki et al. (PACS-CS Collaboration), Phys. Rev. **D79**, 034503 (2009).
 - [16] M. Lüscher, JHEP **0305**, 052 (2003).
 - [17] M. Lüscher, Comput. Phys. Commun. **165**, 199 (2005).

- [18] K.-I. Ishikawa et al. (PACS-CS Collaboration), PoS **LAT2006**, 027 (2006).
- [19] I. P. Omelyan, I. M. Mryglod, and R. Folk, Comput. Phys. Commun. **151**, 272 (2003).
- [20] T. Takaishi and P. de Forcrand, Phys. Rev. **E73**, 036706 (2006).
- [21] J. E. Beam, Phys. Rev. **158**, 907 (1967).
- [22] M. Bolsterli and E. Jezak, Phys. Rev. **135**, B510 (1964).
- [23] W. Detmold and M. J. Savage, Phys. Rev. **D82**, 014511 (2010).
- [24] T. Doi and M. G. Endres (2012), arXiv:1205.0585 [hep-lat].
- [25] W. Detmold and K. Orginos (2012), arXiv:1207.1452 [hep-lat].
- [26] M. Lüscher, Commun. Math. Phys. **105**, 153 (1986).
- [27] S. R. Beane, P. F. Bedaque, A. Parreno, and M. J. Savage, Phys. Lett. **B585**, 106 (2004).
- [28] S. Sasaki and T. Yamazaki, Phys. Rev. **D74**, 114507 (2006).
- [29] S. R. Beane, W. Detmold, and M. J. Savage, Phys. Rev. **D76**, 074507 (2007).
- [30] J. Bratt et al. (LHPC Collaboration), Phys. Rev. **D82**, 094502 (2010).

TABLE I: Simulation parameters for gauge configuration generation at $(\kappa_{ud}, \kappa_s)=(0.1373316, 0.1367526)$. The definition of parameters is same as in Ref. [15].

$L^3 \times T$	$32^3 \times 48$	$40^3 \times 48$	$48^3 \times 48$	$64^3 \times 64$
# run	1	1	1	2
(N_0, N_1, N_2)	(2,2,10)	(2,2,15)	(2,2,16)	(2,2,18)
Block size	$8^3 \times 6$	$10^3 \times 6$	$12^2 \times 6^2$	$8^3 \times 4$
N_{poly}	260	320	320	340
MD time	4000	2000	2000	(1090,810)
$P_{\text{acc}}(\text{HMC})$	0.840	0.925	0.916	(0.880,0.867)
$P_{\text{acc}}(\text{GMP})$	0.957	0.969	0.963	(0.978,0.974)

TABLE II: Number of configurations, separation of trajectories between each measurement, bin size in jackknife analysis, number of measurements on each configuration, exponential smearing parameter set (A, B) in Eq. (12), pion mass m_π and nucleon mass m_N are summarized for each lattice size.

L	T	# config.	τ_{sep}	bin size	# meas.	(A, B)	m_π [GeV]	m_N [GeV]
32	48	200	20	10	192	(1.0,0.18)	0.5109(16)	1.318(4)
40	48	200	10	20	192	(0.8,0.22)	0.5095(8)	1.314(4)
48	48	200	10	20	192	(0.8,0.23)	0.5117(9)	1.320(3)
64	64	190	10	19	256	(0.8,0.23)	0.5119(4)	1.318(2)

TABLE III: Energy shift $-\Delta E_L$ in physical units and fit range for ^4He and ^3He channels on each spatial volume. Extrapolated results in the infinite spatial volume limit are also presented. The first and second errors are statistical and systematic, respectively.

L	^4He		^3He	
	$-\Delta E_L$ [MeV]	fit range	$-\Delta E_L$ [MeV]	fit range
32	47(24)(5)	10–14	23.2(7.6)(1.4)	10–14
40	30(15)(23)	9–13	20.2(6.9)(2.8)	9–14
48	39(20)(27)	10–14	25.5(5.3)(1.7)	10–14
64	46(11)(8)	10–14	19.5(3.7)(1.2)	9–14
∞	43(12)(8)	—	20.3(4.0)(2.0)	—

TABLE IV: Same as Table III for $^3\text{S}_1$ and $^1\text{S}_0$ channels.

L	$^3\text{S}_1$		$^1\text{S}_0$	
	$-\Delta E_L$ [MeV]	fit range	$-\Delta E_L$ [MeV]	fit range
32	12.4(2.1)(0.5)	9–14	6.2(2.4)(0.5)	10–14
40	12.2(1.9)(0.6)	10–15	8.2(4.0)(1.5)	11–15
48	11.1(1.7)(0.3)	10–14	7.3(1.7)(0.5)	10–14
64	11.7(1.2)(0.5)	9–14	7.2(1.4)(0.3)	10–14
∞	11.5(1.1)(0.6)	—	7.4(1.3)(0.6)	—

TABLE V: Energy shift $-\Delta E_L$ in physical units for 3S_1 and 1S_0 channels together with the previous works. The values marked by * are estimated from the scattering length in Ref. [8] employing the leading term of finite volume formula in the $1/L$ expansion [26] with the nucleon mass obtained from the same ensemble in Ref. [30]. The values for Ref. [2] are taken from the results with the \mathcal{O}_1 interpolating operator.

Ref.	quark action	# flavor	m_π [GeV]	L [fm]	$-\Delta E_L$ [MeV]	
					3S_1	1S_0
[7]	Wilson	0	0.72	2.7	29.8(6.9)	14.7(4.3)
		0	0.99	2.7	15.7(6.5)	10.7(4.3)
		0	1.55	2.7	18.1(5.6)	12.2(3.9)
[8]	Mixed (DW on Asqtad)	2+1	0.35	2.5	$-16(19)^*$	$-16(13)^*$
		2+1	0.49	2.5	$-9.5(6.5)^*$	$-15.1(4.2)^*$
		2+1	0.59	2.5	$0.4(2.8)^*$	$0.0(1.1)^*$
[11]	Wilson	0	0.38	4.4	0.97(37)	0.68(26)
		0	0.53	4.4	0.56(11)	0.509(94)
		0	0.73	4.4	0.480(97)	0.400(83)
[2]	Wilson-clover	0	0.80	3.1	10.2(2.2)(1.6)	6.1(2.3)(2.2)
		0	0.80	6.1	9.6(2.6)(0.9)	5.2(2.6)(0.8)
		0	0.80	12.3	7.8(2.1)(0.4)	4.6(2.0)(1.1)
		0	0.80	∞	9.1(1.1)(0.5)	5.5(1.1)(1.0)
[9]	Aniso. Wilson-clover	2+1	0.39	2.4	1.6(2.6)(4.3)	3.9(1.7)(2.6)
[3]	Aniso. Wilson-clover	2+1	0.39	3.0	22.3(2.3)(5.4)	10.4(2.6)(3.1)
		2+1	0.39	3.9	14.9(2.3)(5.8)	8.3(2.2)(3.3)
		2+1	0.39	∞	11(5)(12)	7.1(5.2)(7.3)
[4]	Stout Wilson-clover	2+1	0.81	3.4	25(3)(2)	16(3)(1)
		2+1	0.81	4.5	21(3)(1)	11(2)(1)
		2+1	0.81	6.7	25(3)(2)	19(3)(1)
This work	Wilson-clover	2+1	0.51	2.9	12.4(2.1)(0.5)	6.2(2.4)(0.5)
		2+1	0.51	3.6	12.2(1.9)(0.6)	8.2(4.0)(1.5)
		2+1	0.51	4.3	11.1(1.7)(0.3)	7.3(1.7)(0.5)
		2+1	0.51	5.8	11.7(1.2)(0.5)	7.2(1.4)(0.3)
		2+1 16	0.51	∞	11.5(1.1)(0.6)	7.4(1.3)(0.6)

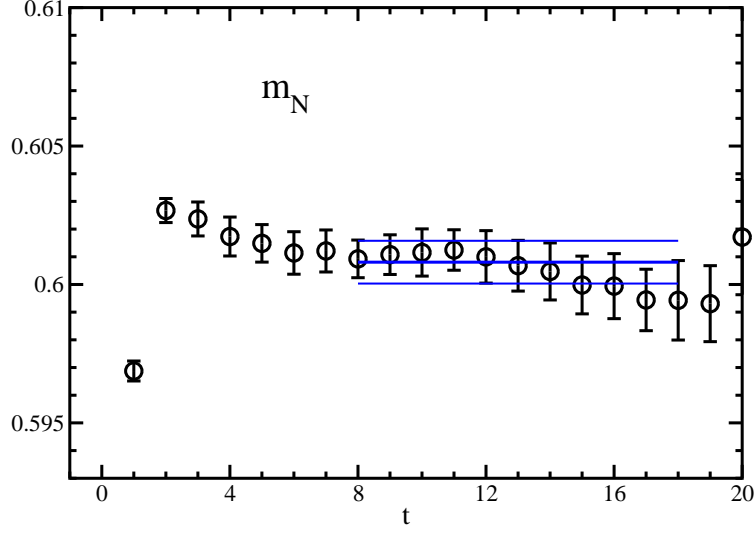


FIG. 1: Nucleon effective mass on $(5.8 \text{ fm})^3$ box in lattice unites. Fit result with one standard deviation error band is expressed by solid lines.

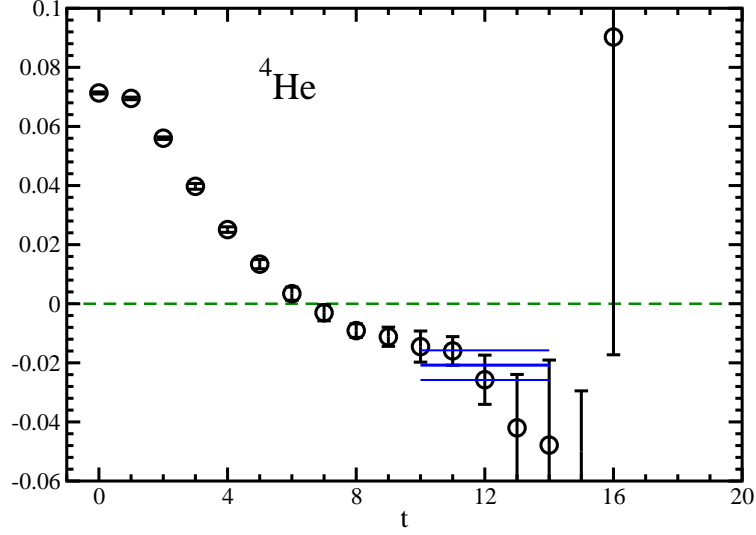


FIG. 2: Effective energy shift ΔE_L^{eff} for ^4He channel on $(5.8 \text{ fm})^3$ box in lattice units. Fit result with one standard deviation error band is expressed by solid lines.

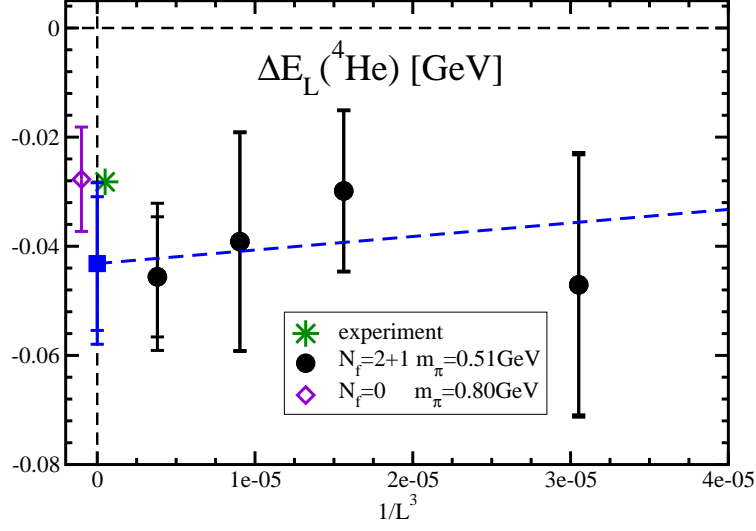


FIG. 3: Spatial volume dependence of ΔE_L in GeV units for ${}^4\text{He}$ channel. Outer bar denotes the combined error of statistical and systematic ones added in quadrature. Inner bar is for the statistical error. Extrapolated result in the infinite spatial volume limit is shown by filled square symbol together with the fit line (dashed). Experimental value (star) and quenched result (open diamond) are also presented.

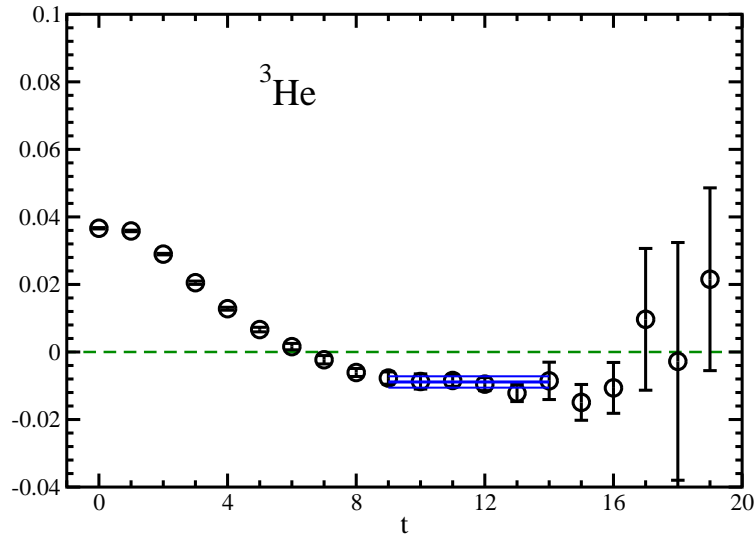


FIG. 4: Same as Fig. 2 for ${}^3\text{He}$ channel.

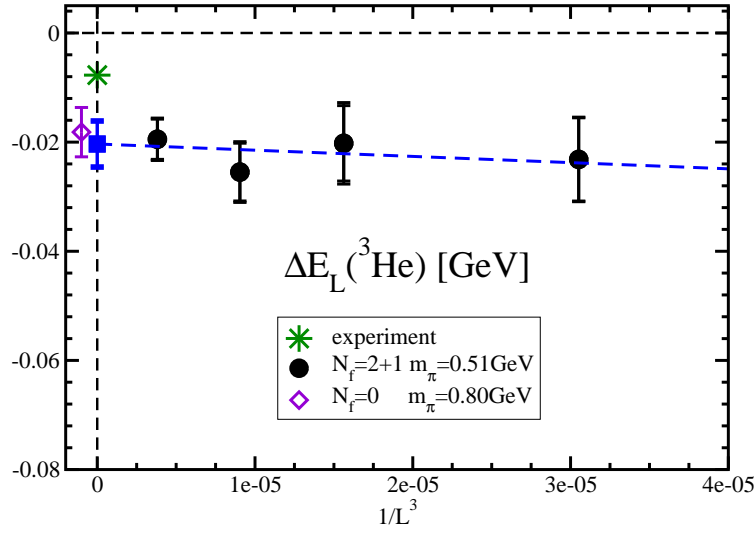


FIG. 5: Same as Fig. 3 for ^3He channel.

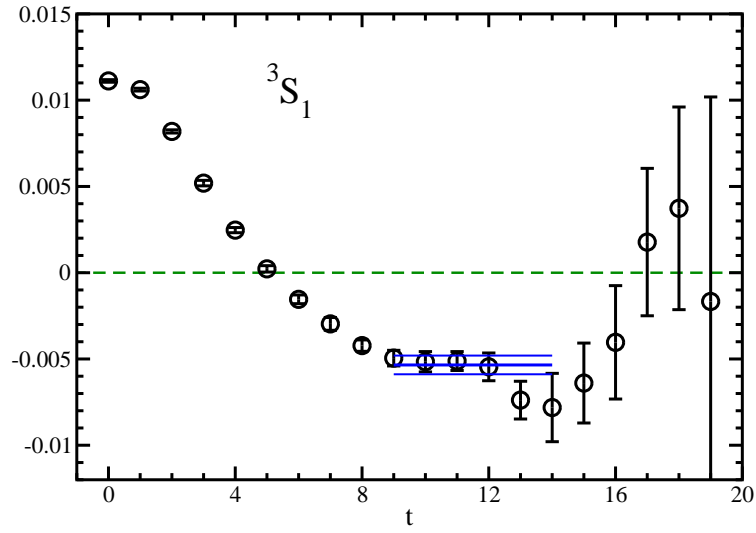


FIG. 6: Same as Fig. 2 for 3S_1 channel.

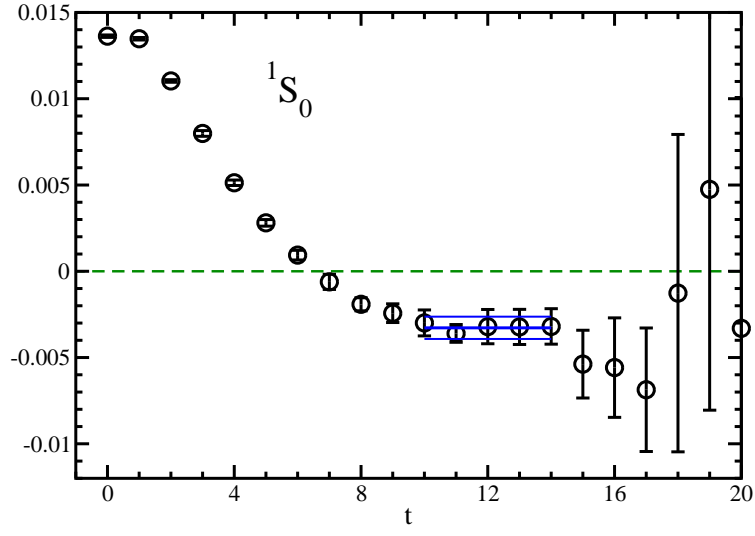


FIG. 7: Same as Fig. 2 for 1S_0 channel.

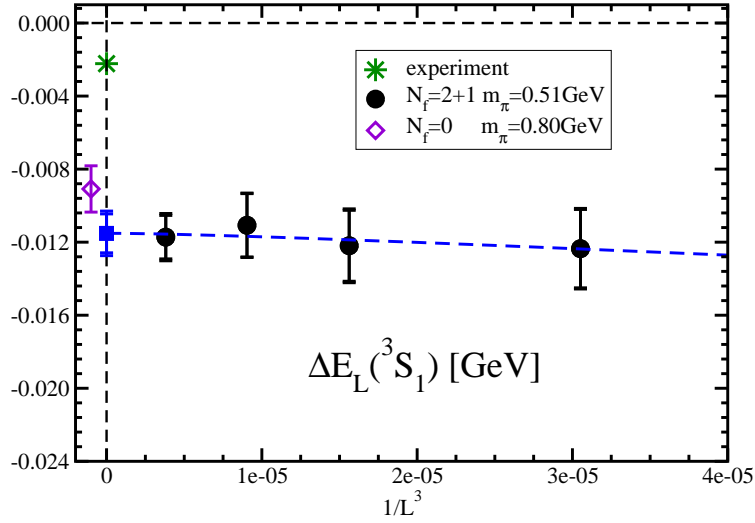


FIG. 8: Same as Fig. 3 for 3S_1 channel.

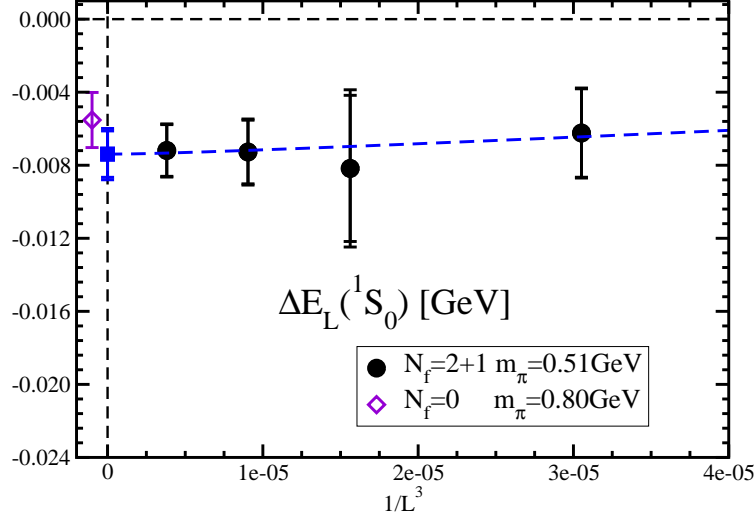


FIG. 9: Same as Fig. 3 for 1S_0 channel.

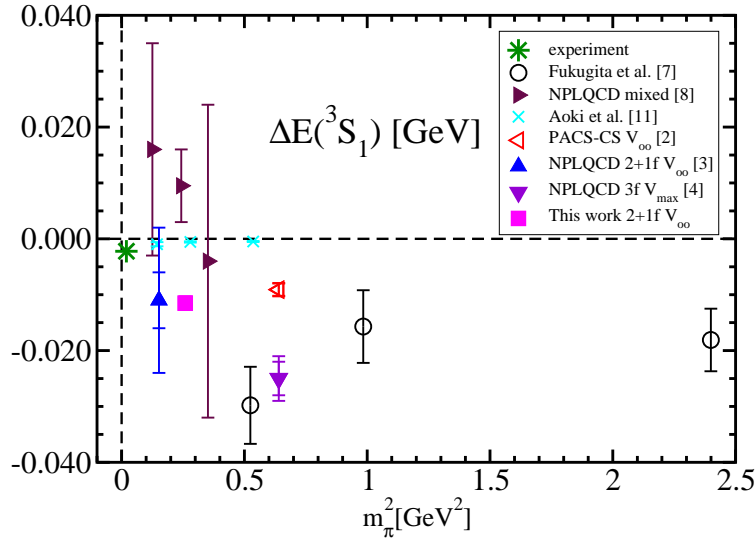


FIG. 10: m_π^2 dependence of ΔE_∞ for 3S_1 channel. Closed(open and cross) symbol denote the 2+1/3 flavor(quenched) result. The results of Refs. [2, 3] and this work are extrapolated values in the infinite volume limit. Experimental result (star) is also presented for comparison.

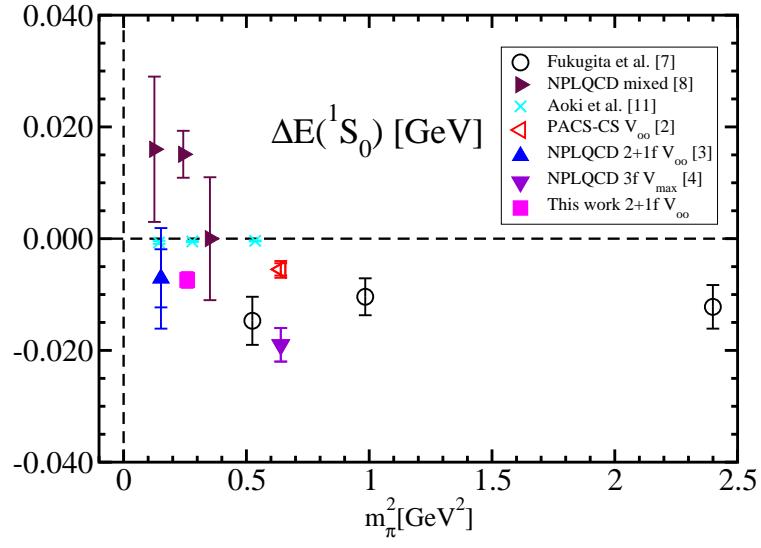


FIG. 11: Same as Fig. 10 for 1S_0 channel.